

Search for Gravitational Waves from Low Mass Compact Binary Coalescence in LIGO's Sixth Science Run and Virgo's Science Runs 2 and 3

J. Abadie¹, B. P. Abbott¹, R. Abbott¹, T. D. Abbott², M. Abernathy³, T. Accadia⁴, F. Acernese^{5a,5c}, C. Adams⁶, R. Adhikari¹, C. Affeldt^{7,8}, M. Agathos^{9a}, P. Ajith¹, B. Allen^{7,10,8}, G. S. Allen¹¹, E. Amador Ceron¹⁰, D. Amariutei¹², R. S. Amin¹³, S. B. Anderson¹, W. G. Anderson¹⁰, K. Arai¹, M. A. Arain¹², M. C. Araya¹, S. M. Aston¹⁴, P. Astone^{15a}, D. Atkinson¹⁶, P. Aufmuth^{8,7}, C. Aulbert^{7,8}, B. E. Aylott¹⁴, S. Babak¹⁷, P. Baker¹⁸, G. Ballardín¹⁹, S. Ballmer²⁰, D. Barker¹⁶, F. Barone^{5a,5c}, B. Barr³, P. Barriga²¹, L. Barsotti²², M. Barsuglia²³, M. A. Barton¹⁶, I. Bartos²⁴, R. Bassiri³, M. Bastarrika³, A. Basti^{25a,25b}, J. Batch¹⁶, J. Bauchrowitz^{7,8}, Th. S. Bauer^{9a}, M. Bebronne⁴, B. Behnke¹⁷, M.G. Beker^{9a}, A. S. Bell³, A. Belletoile⁴, I. Belopolski²⁴, M. Benacquista²⁶, J. M. Berliner¹⁶, A. Bertolini^{7,8}, J. Betzwieser¹, N. Beveridge³, P. T. Beyersdorf²⁷, I. A. Bilenko²⁸, G. Billingsley¹, J. Birch⁶, R. Biswas²⁶, M. Bitossi^{25a}, M. A. Bizouard^{29a}, E. Black¹, J. K. Blackburn¹, L. Blackburn³⁰, D. Blair²¹, B. Bland¹⁶, M. Blom^{9a}, O. Bock^{7,8}, T. P. Bodiya²², C. Bogan^{7,8}, R. Bondarescu³¹, F. Bondu^{32b}, L. Bonelli^{25a,25b}, R. Bonnand³³, R. Bork¹, M. Born^{7,8}, V. Boschi^{25a}, S. Bose³⁴, L. Bosi^{35a}, B. Bouhou²³, S. Braccini^{25a}, C. Bradaschia^{25a}, P. R. Brady¹⁰, V. B. Braginsky²⁸, M. Branchesi^{36a,36b}, J. E. Brau³⁷, J. Breyer^{7,8}, T. Briant³⁸, D. O. Bridges⁶, A. Brillet^{32a}, M. Brinkmann^{7,8}, V. Brisson^{29a}, M. Britzger^{7,8}, A. F. Brooks¹, D. A. Brown²⁰, A. Brummit³⁹, T. Bulik^{40b,40c}, H. J. Bulten^{9a,9b}, A. Buonanno⁴¹, J. Burguet-Castell¹⁰, O. Burmeister^{7,8}, D. Buskulic⁴, C. Buy²³, R. L. Byer¹¹, L. Cadonati⁴², G. Cagnoli^{36a}, E. Calloni^{5a,5b}, J. B. Camp³⁰, P. Campsie³, J. Cannizzo³⁰, K. Cannon⁴³, B. Canuel¹⁹, J. Cao⁴⁴, C. D. Capano²⁰, F. Carbognani¹⁹, S. Caride⁴⁵, S. Caudill¹³, M. Cavaglia⁴⁶, F. Cavalier^{29a}, R. Cavalieri¹⁹, G. Cella^{25a}, C. Cepeda¹, E. Cesarini^{36b}, O. Chaibi^{32a}, T. Chalermongsak¹, E. Chalkley¹⁴, P. Charlton⁴⁷, E. Chassande-Mottin²³, S. Chelkowski¹⁴, Y. Chen⁴⁸, A. Chincarini⁴⁹, A. Chiummo¹⁹, H. Cho⁵⁰, N. Christensen⁵¹, S. S. Y. Chua⁵², C. T. Y. Chung⁵³, S. Chung²¹, G. Ciani¹², F. Clara¹⁶, D. E. Clark¹¹, J. Clark⁵⁴, J. H. Clayton¹⁰, F. Cleva^{32a}, E. Coccia^{55a,55b}, P.-F. Cohadon³⁸, C. N. Colacino^{25a,25b}, J. Colas¹⁹, A. Colla^{15a,15b}, M. Colombini^{15b}, A. Conte^{15a,15b}, R. Conte⁵⁶, D. Cook¹⁶, T. R. Corbitt²², M. Cordier²⁷, N. Cornish¹⁸, A. Corsi¹, C. A. Costa¹³, M. Coughlin⁵¹, J.-P. Coulon^{32a}, P. Couvares²⁰, D. M. Coward²¹, D. C. Coyne¹, J. D. E. Creighton¹⁰, T. D. Creighton²⁶, A. M. Cruise¹⁴, A. Cumming³, L. Cunningham³, E. Cuoco¹⁹, R. M. Cutler¹⁴, K. Dahl^{7,8}, S. L. Danilishin²⁸, R. Dannenberg¹, S. D'Antonio^{55a}, K. Danzmann^{7,8}, V. Dattilo¹⁹, B. Daudert¹, H. Daveloza²⁶, M. Davier^{29a}, G. Davies⁵⁴, E. J. Daw⁵⁷, R. Day¹⁹, T. Dayanga³⁴, R. De Rosa^{5a,5b}, D. DeBra¹¹, G. Debreczeni⁵⁸, J. Degallaix^{7,8}, W. Del Pozzo^{9a}, M. del Prete^{59b}, T. Dent⁵⁴, V. Dergachev¹, R. DeRosa¹³, R. DeSalvo¹, S. Dhurandhar⁶⁰, L. Di Fiore^{5a}, A. Di Lieto^{25a,25b}, I. Di Palma^{7,8}, M. Di Paolo Emilio^{55a,55c}, A. Di Virgilio^{25a}, M. Díaz²⁶, A. Dietz⁴, J. DiGiuglielmo^{7,8}, F. Donovan²², K. L. Dooley¹², S. Dorsher⁶¹, M. Drago^{59a,59b}, R. W. P. Drever⁶², J. C. Driggers¹, Z. Du⁴⁴, J.-C. Dumas²¹, S. Dwyer²², T. Eberle^{7,8}, M. Edgar³, M. Edwards⁵⁴, A. Effler¹³, P. Ehrens¹, G. Endrőczy⁵⁸, R. Engel¹, T. Etzel¹, K. Evans³, M. Evans²², T. Evans⁶, M. Factourovich²⁴, V. Fafone^{55a,55b}, S. Fairhurst⁵⁴, Y. Fan²¹, B. F. Farr⁶³, W. Farr⁶³, D. Fazi⁶³, H. Fehrmann^{7,8}, D. Feldbaum¹², I. Ferrante^{25a,25b}, F. Fidecaro^{25a,25b}, L. S. Finn³¹, I. Fiori¹⁹, R. P. Fisher³¹, R. Flaminio³³, M. Flanigan¹⁶, S. Foley²², E. Forsi⁶, L. A. Forte^{5a}, N. Fotopoulos¹, J.-D. Fournier^{32a}, J. Franc³³, S. Frasca^{15a,15b}, F. Frasconi^{25a}, M. Frede^{7,8}, M. Frei⁶⁴, Z. Frei⁶⁵, A. Freise¹⁴, R. Frey³⁷, T. T. Fricke¹³, D. Friedrich^{7,8}, P. Fritschel²², V. V. Frolov⁶, P. J. Fulda¹⁴, M. Fyffe⁶, M. Galimberti³³, L. Gammaitoni^{35a,35b}, M. R. Ganija⁶⁶, J. Garcia¹⁶, J. A. Garofoli²⁰, F. Garufi^{5a,5b}, M. E. Gáspár⁵⁸, G. Gemme⁴⁹, R. Geng⁴⁴, E. Genin¹⁹, A. Gennai^{25a}, L. Á. Gergely⁶⁷, S. Ghosh³⁴, J. A. Giaime^{13,6}, S. Giampanis¹⁰, K. D. Giardino⁶, A. Giazotto^{25a}, C. Gill³, E. Goetz^{7,8}, L. M. Goggin¹⁰, G. González¹³, M. L. Gorodetsky²⁸, S. Gofler^{7,8}, R. Gouaty⁴, C. Graef^{7,8}, M. Granata²³, A. Grant³, S. Gras²¹, C. Gray¹⁶, N. Gray³, R. J. S. Greenhalgh³⁹, A. M. Gretarsson⁶⁸, C. Greverie^{32a}, R. Grosso²⁶, H. Grote^{7,8}, S. Grunewald¹⁷, G. M. Guidi^{36a,36b}, C. Guido⁶, R. Gupta⁶⁰, E. K. Gustafson¹, R. Gustafson⁴⁵, T. Ha⁶⁹, B. Hage^{8,7}, J. M. Hallam¹⁴, D. Hammer¹⁰, G. Hammond³, J. Hanks¹⁶, C. Hanna^{1,70}, J. Hanson⁶, J. Harms⁶², G. M. Harry²², I. W. Harry⁵⁴, E. D. Harstad³⁷, M. T. Hartman¹², K. Haughian³, K. Hayama⁷¹, J.-F. Hayau^{32b}, J. Heefner¹, A. Heidmann³⁸, M. C. Heintze¹², H. Heitmann³², P. Hello^{29a}, M. A. Hendry³, I. S. Heng³, A. W. Heptonstall¹, V. Herrera¹¹, M. Hewitson^{7,8}, S. Hild³, D. Hoak⁴², K. A. Hodge¹, K. Holt⁶, T. Hong⁴⁸, S. Hooper²¹, D. J. Hosken⁶⁶, J. Hough³, E. J. Howell²¹, B. Hughey¹⁰, S. Husa⁷², S. H. Huttner³, T. Huynh-Dinh⁶, D. R. Ingram¹⁶, R. Inta⁵², T. Isogai⁵¹, A. Ivanov¹, K. Izumi⁷¹, M. Jacobson¹, H. Jang⁷³, P. Jaranowski^{40d}, W. W. Johnson¹³, D. I. Jones⁷⁴, G. Jones⁵⁴, R. Jones³, L. Ju²¹, P. Kalmus¹, V. Kalogera⁶³, I. Kamaretsos⁵⁴, S. Kandhasamy⁶¹, G. Kang⁷³, J. B. Kanner⁴¹, E. Katsavounidis²², W. Katzman⁶, H. Kaufer^{7,8}, K. Kawabe¹⁶, S. Kawamura⁷¹, F. Kawazoe^{7,8},

W. Kells¹, D. G. Keppel¹, Z. Keresztes⁶⁷, A. Khalaidovski^{7,8}, F. Y. Khalili²⁸, E. A. Khazanov⁷⁵, B. Kim⁷³, C. Kim⁷⁶, D. Kim²¹, H. Kim^{7,8}, K. Kim⁷⁷, N. Kim¹¹, Y. -M. Kim⁵⁰, P. J. King¹, M. Kinsey³¹, D. L. Kinzel⁶, J. S. Kissel²², S. Klimenko¹², K. Kokeyama¹⁴, V. Kondrashov¹, R. Kopparapu³¹, S. Koranda¹⁰, W. Z. Korth¹, I. Kowalska^{40b}, D. Kozak¹, V. Kringel^{7,8}, S. Krishnamurthy⁶³, B. Krishnan¹⁷, A. Królak^{40a,40e}, G. Kuehn^{7,8}, R. Kumar³, P. Kwee^{8,7}, P. K. Lam⁵², M. Landry¹⁶, M. Lang³¹, B. Lantz¹¹, N. Lastzka^{7,8}, C. Lawrie³, A. Lazzarini¹, P. Leaci¹⁷, C. H. Lee⁵⁰, H. M. Lee⁷⁸, N. Leindecker¹¹, J. R. Leong^{7,8}, I. Leonor³⁷, N. Leroy^{29a}, N. Letendre⁴, J. Li⁴⁴, T. G. F. Li^{9a}, N. Liguori^{59a,59b}, P. E. Lindquist¹, N. A. Lockerbie⁷⁹, D. Lodhia¹⁴, M. Lorenzini^{36a}, V. Lorette^{29b}, M. Lormand⁶, G. Losurdo^{36a}, J. Luan⁴⁸, M. Lubinski¹⁶, H. Lück^{7,8}, A. P. Lundgren³¹, E. Macdonald³, B. Machenschalk^{7,8}, M. MacInnis²², D. M. Macleod⁵⁴, M. Mageswaran¹, K. Mailand¹, E. Majorana^{15a}, I. Maksimovic^{29b}, N. Man^{32a}, I. Mandel²², V. Mandic⁶¹, M. Mantovani^{25a,25c}, A. Marandi¹¹, F. Marchesoni^{35a}, F. Marion⁴, S. Márka²⁴, Z. Márka²⁴, A. Markosyan¹¹, E. Maros¹, J. Marque¹⁹, F. Martelli^{36a,36b}, I. W. Martin³, R. M. Martin¹², J. N. Marx¹, K. Mason²², A. Masserot⁴, F. Matichard²², L. Matone²⁴, R. A. Matzner⁶⁴, N. Mavalvala²², G. Mazzolo^{7,8}, R. McCarthy¹⁶, D. E. McClelland⁵², S. C. McGuire⁸⁰, G. McIntyre¹, J. McIver⁴², D. J. A. McKechnan⁵⁴, G. D. Meadors⁴⁵, M. Mehmet^{7,8}, T. Meier^{8,7}, A. Melatos⁵³, A. C. Melissinos⁸¹, G. Mendell¹⁶, D. Menendez³¹, R. A. Mercer¹⁰, S. Meshkov¹, C. Messenger⁵⁴, M. S. Meyer⁶, H. Miao²¹, C. Michel³³, L. Milano^{5a,5b}, J. Miller⁵², Y. Minenkov^{55a}, V. P. Mitrofanov²⁸, G. Mitselmakher¹², R. Mittleman²², O. Miyakawa⁷¹, B. Moe¹⁰, P. Moesta¹⁷, M. Mohan¹⁹, S. D. Mohanty²⁶, S. R. P. Mohapatra⁴², D. Moraru¹⁶, G. Moreno¹⁶, N. Morgado³³, A. Morgia^{55a,55b}, T. Mori⁷¹, S. Mosca^{5a,5b}, K. Mossavi^{7,8}, B. Mours⁴, C. M. Mow-Lowry⁵², C. L. Mueller¹², G. Mueller¹², S. Mukherjee²⁶, A. Mullavey⁵², H. Müller-Ebhardt^{7,8}, J. Munch⁶⁶, D. Murphy²⁴, P. G. Murray³, A. Mytidis¹², T. Nash¹, L. Naticchioni^{15a,15b}, R. Nawrodt³, V. Necula¹², J. Nelson³, G. Newton³, A. Nishizawa⁷¹, F. Nocera¹⁹, D. Nolting⁶, L. Nuttall⁵⁴, E. Ochsner⁴¹, J. O'Dell³⁹, E. Oelker²², G. H. Ogin¹, J. J. Oh⁶⁹, S. H. Oh⁶⁹, R. G. Oldenburg¹⁰, B. O'Reilly⁶, R. O'Shaughnessy¹⁰, C. Osthelder¹, C. D. Ott⁴⁸, D. J. Ottaway⁶⁶, R. S. Ottens¹², H. Overmier⁶, B. J. Owen³¹, A. Page¹⁴, G. Pagliaroli^{55a,55c}, L. Palladino^{55a,55c}, C. Palomba^{15a}, Y. Pan⁴¹, C. Pankow¹², F. Paoletti^{25a,19}, M. A. Papa^{17,10}, M. Parisi^{5a,5b}, A. Pasqualetti¹⁹, R. Passaquieti^{25a,25b}, D. Passuello^{25a}, P. Patel¹, M. Pedraza¹, P. Peiris⁸², L. Pekowsky²⁰, S. Penn⁸³, C. Peralta¹⁷, A. Perreca²⁰, G. Persichetti^{5a,5b}, M. Phelps¹, M. Pickenpack^{7,8}, F. Piergiorganni^{36a,36b}, M. Pietka^{40d}, L. Pinard³³, I. M. Pinto⁸⁴, M. Pitkin³, H. J. Pletsch^{7,8}, M. V. Plissi³, R. Poggiani^{25a,25b}, J. Pöld^{7,8}, F. Postiglione⁵⁶, M. Prato⁴⁹, V. Predoi⁵⁴, L. R. Price¹, M. Prijatelj^{7,8}, M. Principe⁸⁴, S. Privitera¹, R. Prix^{7,8}, G. A. Prodi^{59a,59b}, L. Prokhorov²⁸, O. Puncken^{7,8}, M. Punturo^{35a}, P. Puppò^{15a}, V. Quetschke²⁶, F. J. Raab¹⁶, D. S. Rabeling^{9a,9b}, I. Rácz⁵⁸, H. Radkins¹⁶, P. Raffai⁶⁵, M. Rakhmanov²⁶, C. R. Ramet⁶, B. Rankins⁴⁶, P. Rapagnani^{15a,15b}, V. Raymond⁶³, V. Re^{55a,55b}, K. Redwine²⁴, C. M. Reed¹⁶, T. Reed⁸⁵, T. Regimbau^{32a}, S. Reid³, D. H. Reitze¹², F. Ricci^{15a,15b}, R. Riesen⁶, K. Riles⁴⁵, N. A. Robertson^{1,3}, F. Robinet^{29a}, C. Robinson⁵⁴, E. L. Robinson¹⁷, A. Rocchi^{55a}, S. Roddy⁶, C. Rodriguez⁶³, M. Rodruck¹⁶, L. Rolland⁴, J. Rollins²⁴, J. D. Romano²⁶, R. Romano^{5a,5c}, J. H. Romie⁶, D. Rosińska^{40c,40f}, C. Röver^{7,8}, S. Rowan³, A. Rüdiger^{7,8}, P. Ruggi¹⁹, K. Ryan¹⁶, H. Ryll^{7,8}, P. Sainathan¹², M. Sakosky¹⁶, F. Salemi^{7,8}, A. Sambrowski^{7,8}, L. Sammut⁵³, L. Sancho de la Jordana⁷², V. Sandberg¹⁶, S. Sankar²², V. Sannibale¹, L. Santamaría¹, I. Santiago-Prieto³, G. Santostasi⁸⁶, B. Sassolas³³, B. Sathyaprakash⁵⁴, S. Sato⁷¹, P. R. Saulson²⁰, R. L. Savage¹⁶, R. Schilling^{7,8}, S. Schlamminger⁸⁷, R. Schnabel^{7,8}, R. M. S. Schofield³⁷, B. Schulz^{7,8}, B. F. Schutz^{17,54}, P. Schwinberg¹⁶, J. Scott³, S. M. Scott⁵², A. C. Searle¹, F. Seifert¹, D. Sellers⁶, A. S. Sengupta¹, D. Sentenac¹⁹, A. Sergeev⁷⁵, D. A. Shaddock⁵², M. Shaltev^{7,8}, B. Shapiro²², P. Shawhan⁴¹, D. H. Shoemaker²², A. Sibley⁶, X. Siemens¹⁰, D. Sigg¹⁶, A. Singer¹, L. Singer¹, A. M. Sintes⁷², G. Skelton¹⁰, B. J. J. Slagmolen⁵², J. Slutsky¹³, J. R. Smith², M. R. Smith¹, N. D. Smith²², R. J. E. Smith¹⁴, K. Somiya⁴⁸, B. Sorazu³, J. Soto²², F. C. Speirits³, L. Sperandio^{55a,55b}, M. Stefszky⁵², A. J. Stein²², E. Steinert¹⁶, J. Steinlechner^{7,8}, S. Steinlechner^{7,8}, S. Steplewski³⁴, A. Stochino¹, R. Stone²⁶, K. A. Strain³, S. Strigin²⁸, A. S. Stroerer²⁶, R. Sturani^{36a,36b}, A. L. Stuver⁶, T. Z. Summerscales⁸⁸, M. Sung¹³, S. Susmithan²¹, P. J. Sutton⁵⁴, B. Swinkels¹⁹, M. Tacca¹⁹, L. Taffarelo^{59c}, D. Talukder³⁴, D. B. Tanner¹², S. P. Tarabrin^{7,8}, J. R. Taylor^{7,8}, R. Taylor¹, P. Thomas¹⁶, K. A. Thorne⁶, K. S. Thorne⁴⁸, E. Thrane⁶¹, A. Thüring^{8,7}, C. Titsler³¹, K. V. Tokmakov⁷⁹, A. Toncelli^{25a,25b}, M. Tonelli^{25a,25b}, O. Torre^{25a,25c}, C. Torres⁶, C. I. Torrie^{1,3}, E. Tournefier⁴, F. Travasso^{35a,35b}, G. Traylor⁶, M. Trias⁷², K. Tseng¹¹, D. Ugolini⁸⁹, K. Urbanek¹¹, H. Vahlbruch^{8,7}, G. Vajente^{25a,25b}, M. Vallisneri⁴⁸, J. F. J. van den Brand^{9a,9b}, C. Van Den Broeck^{9a}, S. van der Putten^{9a}, A. A. van Veggel³, S. Vass¹, M. Vasuth⁵⁸, R. Vaulin²², M. Vavoulidis^{29a}, A. Vecchio¹⁴, G. Vedovato^{59c}, J. Veitch⁵⁴, P. J. Veitch⁶⁶, C. Veltkamp^{7,8}, D. Verkindt⁴, F. Vetrano^{36a,36b}, A. Viceré^{36a,36b}, A. E. Villar¹, J.-Y. Vinet^{32a}, S. Vitale⁶⁸, S. Vitale^{9a}, H. Vocca^{35a}, C. Vorvick¹⁶, S. P. Vyatchanin²⁸, A. Wade⁵², S. J. Waldman²², L. Wallace¹, Y. Wan⁴⁴, X. Wang⁴⁴, Z. Wang⁴⁴, A. Wanner^{7,8}, R. L. Ward²³, M. Was^{29a}, P. Wei²⁰,

M. Weinert^{7,8}, A. J. Weinstein¹, R. Weiss²², L. Wen^{48,21}, S. Wen⁶, P. Wessels^{7,8}, M. West²⁰, T. Westphal^{7,8}, K. Wette^{7,8}, J. T. Whelan⁸², S. E. Whitcomb^{1,21}, D. White⁵⁷, B. F. Whiting¹², C. Wilkinson¹⁶, P. A. Willems¹, H. R. Williams³¹, L. Williams¹², B. Willke^{7,8}, L. Winkelmann^{7,8}, W. Winkler^{7,8}, C. C. Wipf²², A. G. Wiseman¹⁰, H. Wittel^{7,8}, G. Woan³, R. Wooley⁶, J. Worden¹⁶, J. Yablon⁶³, I. Yakushin⁶, H. Yamamoto¹, K. Yamamoto^{7,8}, H. Yang⁴⁸, D. Yeaton-Massey¹, S. Yoshida⁹⁰, P. Yu¹⁰, M. Yvert⁴, A. Zadrożny^{40e}, M. Zanolin⁶⁸, J.-P. Zendi^{59c}, F. Zhang⁴⁴, L. Zhang¹, W. Zhang⁴⁴, Z. Zhang²¹, C. Zhao²¹, N. Zotov⁸⁵, M. E. Zucker²², and J. Zweigig¹

(*The LIGO Scientific Collaboration and †The Virgo Collaboration)

¹LIGO - California Institute of Technology, Pasadena, CA 91125, USA*

²California State University Fullerton, Fullerton CA 92831 USA*

³SUPA, University of Glasgow, Glasgow, G12 8QQ, United Kingdom*

⁴Laboratoire d'Annecy-le-Vieux de Physique des Particules (LAPP),

Université de Savoie, CNRS/IN2P3, F-74941 Annecy-Le-Vieux, France†

⁵INFN, Sezione di Napoli ^a; Università di Napoli 'Federico II' ^b Complesso Universitario di Monte S. Angelo, I-80126 Napoli; Università di Salerno, Fisciano, I-84084 Salerno ^c, Italy†

⁶LIGO - Livingston Observatory, Livingston, LA 70754, USA*

⁷Albert-Einstein-Institut, Max-Planck-Institut für Gravitationsphysik, D-30167 Hannover, Germany*

⁸Leibniz Universität Hannover, D-30167 Hannover, Germany*

⁹Nikhef, Science Park, Amsterdam, the Netherlands^a; VU University Amsterdam, De Boelelaan 1081, 1081 HV Amsterdam, the Netherlands^b†

¹⁰University of Wisconsin-Milwaukee, Milwaukee, WI 53201, USA*

¹¹Stanford University, Stanford, CA 94305, USA*

¹²University of Florida, Gainesville, FL 32611, USA*

¹³Louisiana State University, Baton Rouge, LA 70803, USA*

¹⁴University of Birmingham, Birmingham, B15 2TT, United Kingdom*

¹⁵INFN, Sezione di Roma^a; Università 'La Sapienza'^b, I-00185 Roma, Italy†

¹⁶LIGO - Hanford Observatory, Richland, WA 99352, USA*

¹⁷Albert-Einstein-Institut, Max-Planck-Institut für Gravitationsphysik, D-14476 Golm, Germany*

¹⁸Montana State University, Bozeman, MT 59717, USA*

¹⁹European Gravitational Observatory (EGO), I-56021 Cascina (PI), Italy†

²⁰Syracuse University, Syracuse, NY 13244, USA*

²¹University of Western Australia, Crawley, WA 6009, Australia*

²²LIGO - Massachusetts Institute of Technology, Cambridge, MA 02139, USA*

²³Laboratoire AstroParticule et Cosmologie (APC) Université Paris Diderot, CNRS: IN2P3, CEA: DSM/IRFU, Observatoire de Paris, 10 rue A.Domon et L.Duquet, 75013 Paris - France†

²⁴Columbia University, New York, NY 10027, USA*

²⁵INFN, Sezione di Pisa^a; Università di Pisa^b; I-56127 Pisa; Università di Siena, I-53100 Siena^c, Italy†

²⁶The University of Texas at Brownsville and Texas Southmost College, Brownsville, TX 78520, USA*

²⁷San Jose State University, San Jose, CA 95192, USA*

²⁸Moscow State University, Moscow, 119992, Russia*

²⁹LAL, Université Paris-Sud, IN2P3/CNRS, F-91898 Orsay^a; ESPCI, CNRS, F-75005 Paris^b, France†

³⁰NASA/Goddard Space Flight Center, Greenbelt, MD 20771, USA*

³¹The Pennsylvania State University, University Park, PA 16802, USA*

³²Université Nice-Sophia-Antipolis, CNRS, Observatoire de la Côte d'Azur,

F-06304 Nice^a; Institut de Physique de Rennes, CNRS,

Université de Rennes 1, 35042 Rennes^b, France†

³³Laboratoire des Matériaux Avancés (LMA), IN2P3/CNRS, F-69622 Villeurbanne, Lyon, France†

³⁴Washington State University, Pullman, WA 99164, USA*

³⁵INFN, Sezione di Perugia^a; Università di Perugia^b, I-06123 Perugia, Italy†

³⁶INFN, Sezione di Firenze, I-50019 Sesto Fiorentino^a; Università degli Studi di Urbino 'Carlo Bo', I-61029 Urbino^b, Italy†

³⁷University of Oregon, Eugene, OR 97403, USA*

³⁸Laboratoire Kastler Brossel, ENS, CNRS, UPMC,

Université Pierre et Marie Curie, 4 Place Jussieu, F-75005 Paris, France†

³⁹Rutherford Appleton Laboratory, HSIC, Chilton, Didcot, Oxon OX11 0QX United Kingdom*

⁴⁰IM-PAN 00-956 Warsaw^a; Astronomical Observatory Warsaw University 00-478 Warsaw^b; CAMK-PAN 00-716 Warsaw^c; Białystok University 15-424 Białystok^d; IPJ 05-400 Świerk-Otwock^e; Institute of Astronomy 65-265 Zielona Góra^f, Poland†

⁴¹University of Maryland, College Park, MD 20742 USA*

⁴²University of Massachusetts - Amherst, Amherst, MA 01003, USA*

⁴³Canadian Institute for Theoretical Astrophysics,

University of Toronto, Toronto, Ontario, M5S 3H8, Canada*

⁴⁴Tsinghua University, Beijing 100084 China*

⁴⁵University of Michigan, Ann Arbor, MI 48109, USA*

- ⁴⁶The University of Mississippi, University, MS 38677, USA*
- ⁴⁷Charles Sturt University, Wagga Wagga, NSW 2678, Australia*
- ⁴⁸Caltech-CaRT, Pasadena, CA 91125, USA*
- ⁴⁹INFN, Sezione di Genova; I-16146 Genova, Italy[†]
- ⁵⁰Pusan National University, Busan 609-735, Korea*
- ⁵¹Carleton College, Northfield, MN 55057, USA*
- ⁵²Australian National University, Canberra, ACT 0200, Australia*
- ⁵³The University of Melbourne, Parkville, VIC 3010, Australia*
- ⁵⁴Cardiff University, Cardiff, CF24 3AA, United Kingdom*
- ⁵⁵INFN, Sezione di Roma Tor Vergata^a; Università di Roma Tor Vergata, I-00133 Roma^b; Università dell'Aquila, I-67100 L'Aquila^c, Italy[†]
- ⁵⁶University of Salerno, I-84084 Fisciano (Salerno), Italy and INFN (Sezione di Napoli), Italy[†]
- ⁵⁷The University of Sheffield, Sheffield S10 2TN, United Kingdom*
- ⁵⁸RMKI, H-1121 Budapest, Konkoly Thege Miklós út 29-33, Hungary*
- ⁵⁹INFN, Gruppo Collegato di Trento^a and Università di Trento^b, I-38050 Povo, Trento, Italy; INFN, Sezione di Padova^c and Università di Padova^d, I-35131 Padova, Italy[†]
- ⁶⁰Inter-University Centre for Astronomy and Astrophysics, Pune - 411007, India*
- ⁶¹University of Minnesota, Minneapolis, MN 55455, USA*
- ⁶²California Institute of Technology, Pasadena, CA 91125, USA*
- ⁶³Northwestern University, Evanston, IL 60208, USA*
- ⁶⁴The University of Texas at Austin, Austin, TX 78712, USA*
- ⁶⁵Eötvös Loránd University, Budapest, 1117 Hungary*
- ⁶⁶University of Adelaide, Adelaide, SA 5005, Australia*
- ⁶⁷University of Szeged, 6720 Szeged, Dóm tér 9, Hungary*
- ⁶⁸Embry-Riddle Aeronautical University, Prescott, AZ 86301 USA*
- ⁶⁹National Institute for Mathematical Sciences, Daejeon 305-390, Korea*
- ⁷⁰Perimeter Institute for Theoretical Physics, Ontario, Canada, N2L 2Y5*
- ⁷¹National Astronomical Observatory of Japan, Tokyo 181-8588, Japan*
- ⁷²Universitat de les Illes Balears, E-07122 Palma de Mallorca, Spain*
- ⁷³Korea Institute of Science and Technology Information, Daejeon 305-806, Korea*
- ⁷⁴University of Southampton, Southampton, SO17 1BJ, United Kingdom*
- ⁷⁵Institute of Applied Physics, Nizhny Novgorod, 603950, Russia*
- ⁷⁶Lund Observatory, Box 43, SE-221 00, Lund, Sweden*
- ⁷⁷Hanyang University, Seoul 133-791, Korea*
- ⁷⁸Seoul National University, Seoul 151-742, Korea*
- ⁷⁹University of Strathclyde, Glasgow, G1 1XQ, United Kingdom*
- ⁸⁰Southern University and A&M College, Baton Rouge, LA 70813, USA*
- ⁸¹University of Rochester, Rochester, NY 14627, USA*
- ⁸²Rochester Institute of Technology, Rochester, NY 14623, USA*
- ⁸³Hobart and William Smith Colleges, Geneva, NY 14456, USA*
- ⁸⁴University of Sannio at Benevento, I-82100 Benevento, Italy and INFN (Sezione di Napoli), Italy*
- ⁸⁵Louisiana Tech University, Ruston, LA 71272, USA*
- ⁸⁶McNeese State University, Lake Charles, LA 70609 USA*
- ⁸⁷University of Washington, Seattle, WA, 98195-4290, USA*
- ⁸⁸Andrews University, Berrien Springs, MI 49104 USA*
- ⁸⁹Trinity University, San Antonio, TX 78212, USA*
- ⁹⁰Southeastern Louisiana University, Hammond, LA 70402, USA*

(RCS Id: s6-cbc-lowmass.tex,v 1.81 2011/12/12 17:19:44 cdcapano Exp ; compiled 23 March 2022)

We report on a search for gravitational waves from coalescing compact binaries using LIGO and Virgo observations between July 7, 2009 and October 20, 2010. We searched for signals from binaries with total mass between 2 and 25 M_{\odot} ; this includes binary neutron stars, binary black holes, and binaries consisting of a black hole and neutron star. The detectors were sensitive to systems up to 40 Mpc distant for binary neutron stars, and further for higher mass systems. No gravitational-wave signals were detected. We report upper limits on the rate of compact binary coalescence as a function of total mass, including the results from previous LIGO and Virgo observations. The cumulative 90%-confidence rate upper limits of the binary coalescence of binary neutron star, neutron star–black hole and binary black holes systems are 1.3×10^{-4} , 3.1×10^{-5} and 6.4×10^{-6} $\text{Mpc}^{-3}\text{yr}^{-1}$, respectively. We also report on results from a blind injection challenge.

PACS numbers: 95.85.Sz, 04.80.Nn, 07.05.Kf, 97.60.Jd, 97.60.Lf, 97.80.-d

I. INTRODUCTION

During 2009 and 2010, both the Laser Interferometer Gravitational-wave Observatory (LIGO) [1] and Virgo [2] gravitational-wave detectors undertook science runs with better sensitivity across a broader range of frequencies than previously achieved. Among the most promising sources of gravitational waves for these detectors are compact stellar mass binaries as they spiral in toward each other and merge. For such systems, which include binary neutron stars (BNS), binary black holes (BBH), and neutron star–black hole binaries (NSBH), the late stages of inspiral and merger occur in the most sensitive band (between 40 and 1000 Hz) of the LIGO and Virgo detectors. In this paper, we report on a search for gravitational waves from binary systems with a maximum total mass of $25 M_{\odot}$, and a minimum component mass of $1 M_{\odot}$.

A hardware injection was performed during the data collection without the knowledge of the data analysis teams as part of a “blind injection challenge” [3]. This challenge was intended to test the data analysis procedures and processes for evaluating candidate events. The injection was performed by coherently actuating the mirrors on the LIGO and Virgo detectors to mimic a gravitational-wave signal. Prior to its unveiling as an injection (“unblinding”), the event was determined to be a candidate gravitational wave: it was found to have a false alarm rate of less than 1 in 7,000 years and no evidence for an instrumental or environmental origin could be found. After the analysis of the event was finished it was revealed to be a blind injection and removed from the data.

With the blind injection removed there were no gravitational waves observed above the noise background. As a result we place upper limits on rates of compact binary coalescence (CBC), using upper limits from previous gravitational-wave searches [4] as prior information. The upper limits presented here are up to a factor 1.4 lower than previously derived limits but still two to three orders of magnitude above expected CBC rates [5].

The paper is laid out as follows. In Section II, we provide a brief description of the detectors and their sensitivities during LIGO’s sixth science run (S6) and Virgo’s second and third science runs. In Section III we present a brief overview of the analysis methods used in performing the search. In Section IV we discuss the recovery of the blind injection. In Section V we present the results of the search with the blind injection removed. In Section VI we give the upper limits obtained from the search and close with a brief discussion in Section VII.

II. DETECTORS

The LIGO observatory comprises two sites, one in Hanford, WA and the second in Livingston, LA. The data used in this search were taken during S6, which took

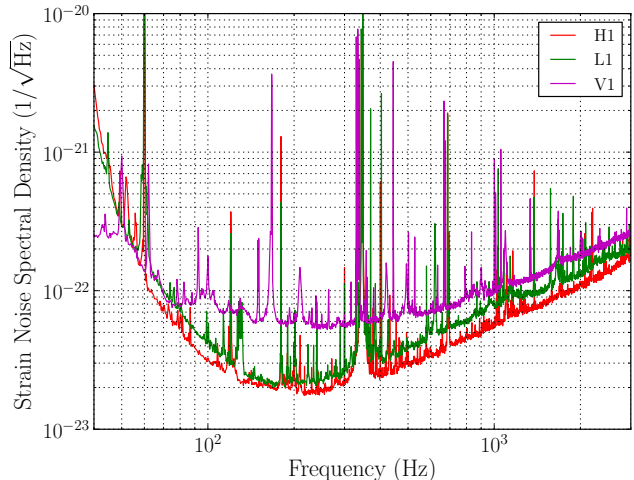


FIG. 1: Typical detector strain noise spectral density for the LIGO S6 and Virgo VSR2/3 runs. From lowest to highest at 10^2 Hz, the curves are for the H1, L1 and V1 detectors.

place between 7 July 2009 and 20 October 2010. During S6 each of these sites operated a single 4km laser interferometer, denoted as H1 and L1 respectively. The 2km H2 instrument at the Hanford site which operated in earlier science runs was not operational in S6. Following LIGO’s fifth science run (S5) [1], several hardware changes were made to the LIGO detectors so that prototypes of advanced LIGO technology could be installed and tested [6, 7]. This included the installation of a higher power laser, and the implementation of a DC readout system that included a new output mode cleaner on an advanced LIGO seismic isolation table [8]. In addition, the hydraulic seismic isolation system was improved by fine tuning its feed-forward path.

The Virgo detector (denoted V1) is a single, 3km laser interferometer located in Cascina, Italy. The data used in this search were taken from both Virgo’s second science run (VSR2), which ran from 7 July 2009 to 8 January 2010, and its third science run (VSR3), which ran from 11 August 2010 to 20 October 2010. In the period between the first Virgo science run (VSR1) and VSR2, several enhancements were made to the Virgo detector. Specifically, a more powerful laser was installed in Virgo, along with a thermal compensation system and improved scattered light mitigation. During early 2010, monolithic suspensions were installed, which involved replacing Virgo’s test masses with new mirrors hung from fused-silica fibers [9]. VSR3 followed this upgrade.

The sensitivity of the detectors during the S6, VSR2 and VSR3 runs is shown in Figure 1. The corresponding sensitivity to binary coalescence signals is shown in Figure 2. This figure shows the distance at which an optimally oriented and located binary would produce a signal-to-noise ratio (SNR) of 8 in a given detector. The figure illustrates the improvement in sensitivity for the LIGO detectors between S5 and S6 and for Virgo be-

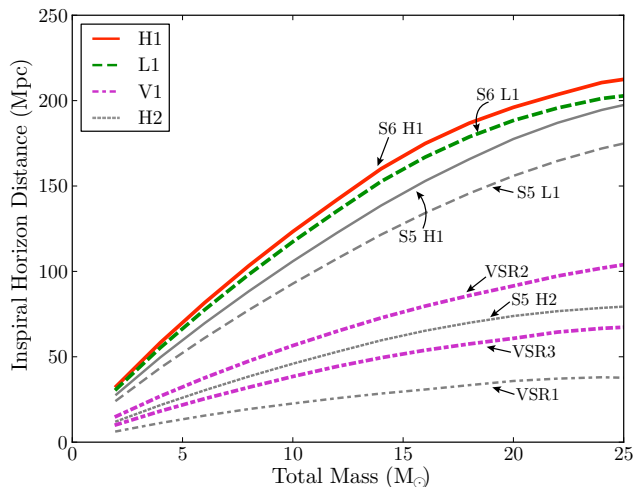


FIG. 2: Inspiral horizon distance versus total mass from S5/VSR1 (gray lines) and S6/VSR2/VSR3 (colored lines). The horizon distance is the distance at which an optimally located and oriented binary would produce an expected signal-to-noise ratio of 8. The figure shows the best sensitivity achieved by each detector during the runs.

tween VSR1 and VSR2. The reduction in the horizon distance of the Virgo detector in VSR3 is due to a mirror with an incorrect radius of curvature being installed during the conversion to monolithic suspension.

III. BINARY COALESCENCE SEARCH

To search for gravitational waves from compact binary coalescence [4, 10, 11], we use matched filtering to correlate the detector’s strain output with a theoretical model of the gravitational waveform [12]. Each detector’s output is separately correlated against a bank [13] of template waveforms generated at 3.5 post-Newtonian order in the frequency domain [14, 15]. Templates were laid out across the mass range such that no more than 3% of the SNR was lost due to the discreteness of the bank. Only non-spinning waveforms with a component mass $\geq 1 M_{\odot}$ were generated, and the templates were terminated prior to merger. In the early stages of the run, as in previous searches [4, 10, 11], the template bank included waveforms from binaries with a total mass $M \leq 35 M_{\odot}$. However, the search results indicated that the higher mass templates ($M > 25 M_{\odot}$) were more susceptible to non-stationary noise in the data. Furthermore, it is at these higher masses where the merger and ringdown phases of the signal come into the detectors’ sensitive bands. Consequently, the upper mass limit of this search was reduced to $25 M_{\odot}$ during the latter stages of the science run. Results of a search for higher mass binary black holes using template waveforms incorporating a full coalescence (inspiral-merger-ringdown) will be presented in a future publication. Although the template waveforms in this search neglect the spin of the binary components, the

search is still capable of detecting binaries whose waveforms are modulated by the effect of spin [16].

We require candidate signals to have a matched filter SNR greater than 5.5 in at least two detectors, and to have consistent values of template masses and time of arrival (allowing for travel-time difference) across the detectors where this threshold is exceeded [17]. We use a chi-squared test [18] to suppress non-Gaussian noise transients, which have a high SNR but whose time-frequency evolution is inconsistent with the template waveform. If the reduced chi-squared χ_r^2 of a signal is greater than unity, we re-weight the SNR ρ in order to suppress the significance of false signals, obtaining a re-weighted SNR statistic

$$\hat{\rho} = \begin{cases} \frac{\rho}{[(1 + (\chi_r^2)^3)/2]^{1/6}} & \text{for } \chi_r^2 > 1, \\ \rho & \text{for } \chi_r^2 \leq 1. \end{cases} \quad (1)$$

Our analysis reports the coalescence time and the quadrature sum, ρ_c , of re-weighted SNRs for events coincident between the detectors. The statistic ρ_c is then used to rank events by their significance above the expected background. To measure the background rate of coincident events in the search, we time-shift data from the detectors by an amount greater than the gravitational-wave travel time difference between detector sites and re-analyze the data. Many independent time-shifts are performed to obtain a good estimate of the probability of accidental coincidence of noise transients at two or more sites. The analysis procedure described above is similar to the one used in previous searches of LIGO and Virgo data, such as [11] and [10].

The background rates of coincident events were initially estimated using 100 time-shifted analyses. These background rates vary depending on the binary’s mass — via the waveform duration and frequency band — and also on the detectors involved in the coincidence (the *event type*). The relevant mass parameter is the binary’s chirp mass, $\mathcal{M} \equiv (m_1 m_2)^{3/5} (m_1 + m_2)^{-1/5}$, where m_1 and m_2 are the component masses in the binary system. Thus, we sort coincident events into three bins by chirp mass, and by event type [10].

The requirement of a coincident signal between at least two sites restricts the times that can be analyzed to four distinct types of *coincident time*. Between July 2009 and October 2010, a total of 0.56 yr of two-or-more-site coincident data was collected. This comprised 0.14 yr of H1L1V1 coincident data, 0.21 yr of H1L1 data, 0.13 yr of H1V1 data, and 0.08 yr of L1V1 data. During H1L1V1 coincident time there are four distinct event types: H1L1V1, H1L1, H1V1, and L1V1. In S6/VSR2, all four event types were kept. In S6/VSR3, H1V1 and L1V1 events in triple-coincident time were discarded due to the heightened rate of transient noise artifacts in Virgo and its decreased sensitivity.

For each candidate, a false alarm rate (FAR) is computed by comparing its ρ_c value to background events in the same mass bin and coincident time and with the

same event type. Candidates' FAR values are then compared to background events in *all* bins and event types, over the appropriate coincident time, to calculate a combined FAR. This is the detection statistic which is used to assess the significance of events over the entire analysis time.

Due to the finite number of time-shifts performed, the smallest non-zero FAR that can be calculated is $1/T_{\text{bg}}$, where T_{bg} is the total background time obtained by summing the coincident live time in each time-shift. If an event was found to be louder than all background events within its analysis period, additional time-shifted analyses were performed to calculate a more precise FAR for the event.

Although the detectors are enclosed in vacuum systems and isolated from vibrational, acoustic and electromagnetic disturbances, their typical output data contains a larger number of transient noise events (glitches) with higher amplitude than expected from Gaussian processes alone. Each observatory is equipped with a system of environmental and instrumental monitors that are sensitive to glitch sources but have a negligible sensitivity to gravitational waves. These sensors were used to identify times when the detector output was potentially corrupted [19–21]. We grouped these times into two categories: periods with well-understood couplings between non-gravitational-wave sources and detector output, and periods when a statistical correlation was found but a coupling mechanism was not identified. In our primary search — which included the identification of gravitational-wave candidates and the calculation of upper limits — we removed (*vetoed*) times that fell in either of the two categories from the analysis, along with any coincident events that occurred during these periods. We also performed a secondary search for possible loud candidate events, in which only the times with known couplings were vetoed.

Approximately 10% of the data, designated *playground*, was used for tuning and data quality investigations. This data was searched for gravitational waves, but not used in calculating upper limits. After all vetoes were applied and playground time excluded, there was 0.09 yr of H1L1V1 time, 0.17 yr of H1L1 time, 0.10 yr of H1V1 time, and 0.07 yr of L1V1 time, giving a total analysis time of 0.43 yr.

A substantial change from the analysis procedure of [11] was that data were analyzed in two-week blocks with a latency of two to four weeks, to allow for feedback of information to ongoing detector characterization efforts and to improve data quality. Thus, during the search many new vetoes were introduced resulting from improved understanding of the detectors. However, significant numbers of delta-function-like glitches with large amplitudes remained unvetoes in the LIGO detectors. These were found to cause artifacts in the matched filter output over a short time surrounding the glitch: thus, during the latter stages of the search, 8 s of time on either side of any matched filter SNR exceeding 250 was

vetoed. Times removed from the primary search by this veto were still examined for possible loud events.

IV. BLIND INJECTION RECOVERY

The search pipeline described above identified a gravitational-wave candidate occurring on 16 September 2010 at 06:42:23 UTC, with $\rho_c = 12.5$ in coincidence between the two LIGO detectors in the middle mass bin $3.48 \leq \mathcal{M}/M_\odot < 7.40$. The highest matched-filter SNR obtained in the search was 15 at $\mathcal{M} = 4.7 M_\odot$ in H1 and 10 at $\mathcal{M} = 4.4 M_\odot$ in L1. This difference in SNRs is consistent with typical differences in antenna response factors for these differently-oriented detectors. Virgo was also operating at the time of the event, but its sensitivity was a factor of approximately four lower than the LIGO detectors; the absence of a signal in Virgo above the single-detector SNR threshold of 5.5 was consistent with this fact. In the LIGO detectors, the signal was louder than all time-shifted H1L1 coincident events in the same mass bin throughout S6. However, with only 100 time-shifts, we could only bound the FAR to $< 1/23$ years, even when folding in all data from the entire analysis. To obtain a better estimate of the event's FAR we performed all possible multiples of 5-second time-shifts on four calendar months of data around the event, corresponding to an effective analysis time of 2.0×10^5 years. We found five events with a value of ρ_c equal to or larger than the candidate's, as shown in Figure 3. These five events were all coincidences between the candidate's signal in H1 and time-shifted transient noise in L1. When we excluded 8 seconds from around the event's time in the background estimation, we found *no* background events with ρ_c greater than the candidate and we obtained a significantly different background distribution, also shown in Figure 3.

Including the events at the time of the candidate in the background estimate, the FAR of the event in the $3.48 \leq \mathcal{M}/M_\odot < 7.40$ mass bin, coincident in the LIGO detectors, was estimated to be 1 in 4×10^4 years. Since this event occurred in H1L1V1 time during VSR3, only two event types were considered: H1L1 double-coincident events and H1L1V1 triple-coincident events. This resulted in a trials factor of 6 (accounting for the three mass bins and two coincidence types) and a combined FAR of 1 in 7,000 years. The false alarm probability of this event in this analysis, over the 0.47 yr of coincident time remaining after all vetoes were applied, was 7×10^{-5} .

We performed an extensive investigation to check for any non-gravitational-wave causes for the observed event. The injection passed all checks performed. We deliberately did not look at the data channel that records injected signals. We performed a thorough study of the coupling of environmental noise to the gravitational-wave channel. None of the environmental monitors recorded a transient during the time of the injection. The LIGO

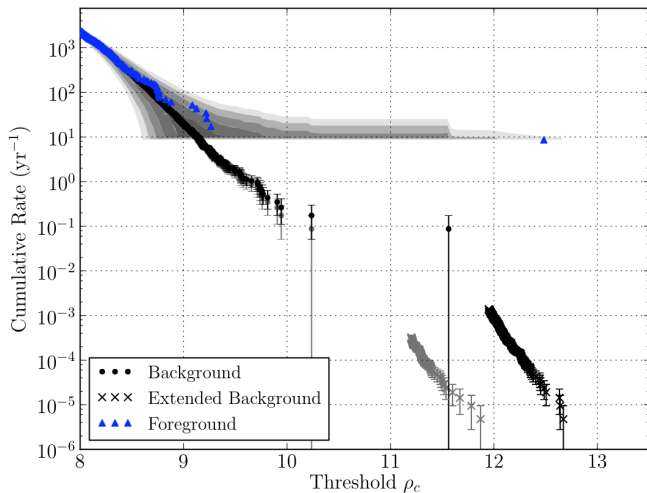


FIG. 3: The cumulative rate of events with chirp mass $3.48 \leq \mathcal{M}/M_{\odot} < 7.40$ coincident in the H1 and L1 detectors, seen in four months of data around the 16 September candidate, as a function of the threshold ranking statistic ρ_c . The blue triangles show coincident events. Black dots show the background estimated from 100 time-shifts. Black crosses show the extended background estimation from all possible 5-second shifts on this data restricted, for computational reasons, to only the tail of loudest events. The gray dots and crosses show the corresponding background estimates when 8 seconds of data around the time of the candidate are excluded. Gray shaded contours show the $1 - 5\sigma$ (dark to light) consistency of coincident events with the estimated background including the extended background estimate, for the events and analysis time shown, including the candidate time. This event was later revealed to have been a blind injection.

observatories were in quiet night-time operation with near maximum astrophysical range; the Virgo detector had quiet environmental conditions, except for elevated micro-seismic levels. Most mechanisms that could cause coincident signals among widely separated detectors were ruled out. It is very unlikely that such mechanisms could cause a signal that monotonically increases in frequency and is visible in the LIGO data without leaving a clear signature in the environmental monitors.

A loud transient occurred in L1 9 seconds before the coalescence time of the signal. That transient belonged to a known family of sharp (~ 10 ms) and loud ($\text{SNR} \approx 200\text{--}80000$) glitches that appear 10–30 times per day in the output optical sensing system of this detector. Since the candidate signal swept through the sensitive band of the detector, from 40 Hz to coalescence, in less than 4 seconds, it did not overlap the loud transient. Studies, including re-analysis of the data with the glitch removed, indicated that the signal was not related to the earlier instrumental glitch. No evidence was found that the observed signal was associated with, or corrupted by, any instrumental effect.

Following the completion of this analysis, the event was revealed to be a blind injection. While the analy-

sis groups did not know the event was an injection prior to its unblinding, they did know that one or more blind injections may be performed during the analysis period. Such blind injections have been carried out before: see [4] for the results of a blind injection performed in a previous run. This event was the only coherent CBC blind injection performed during S6 and VSR2 and 3. The injection was identified as a gravitational-wave candidate with high probability, and the blind injection challenge was considered to be successful [3].

In order to more accurately determine the parameters of the event prior to the unblinding, we performed coherent Bayesian analyses of the data using models of both spinning and non-spinning compact binary objects. These analyses showed evidence for the presence of a weak signal in Virgo, consistent with the signal seen by the two LIGO detectors. The strength of a signal in Virgo is an important input to the localization of a source in the sky. Parameter estimates varied significantly depending on the exact model used for the gravitational waveform, particularly when we included spin effects. However, conservative unions of the confidence intervals from the different waveform models were consistent with most injected parameters, including chirp mass, time of coalescence, and sky location. In addition, the signal was correctly identified as having at least one highly-spinning component with the spin misaligned with the angular orbital momentum. We will describe the details of parameter estimation on this and other CBC injections in a future paper (in preparation).

V. SEARCH RESULTS

After the event was revealed to be a blind injection the data containing it was removed from the analysis. With the injection excluded, there were no gravitational-wave candidates observed in the data. Indeed the search result was consistent with the background estimated from time-shifting the data. The most significant event was an L1V1 event in L1V1 time with a combined FAR of 1.2yr^{-1} . The second and third most significant events had combined FARs of 2.2yr^{-1} and 5.6yr^{-1} , respectively. All of these events were consistent with background: having analyzed ~ 0.5 yr of data, we would expect the loudest event to have a FAR of $2 \pm 2\text{yr}^{-1}$. Although no detection candidates were found, a detailed investigation of the loudest events in each analysis period was performed, to improve our understanding of instrumental data quality.

VI. BINARY COALESCENCE RATE LIMITS

Given the absence of gravitational-wave signals, we used our observations to set upper limits on coalescence rates of BNS, BBH, and NSBH systems. We used the procedure described in [22–24] to compute Bayesian 90%

confidence level upper limits on the coalescence rate for the various systems, making use of previous results [4, 10, 11] as prior information on the rates.

The rate of binary coalescences in a spiral galaxy is expected to be proportional to the star formation rate, and hence blue light luminosity, of the galaxy [25]. Previous searches [4, 10, 11] presented upper limits in terms of blue light luminosity, using units of $L_{10}^{-1}\text{yr}^{-1}$, where one L_{10} is 10^{10} times the solar blue light luminosity. There are, however, numerous challenges to evaluating the upper limit as a function of luminosity, not least due to the large uncertainties in both the luminosity of and distance to nearby galaxies, as well as the lack of a complete galaxy catalogue at larger distances [22, 25]. On large scales (greater than ~ 20 Mpc), the luminosity per unit volume is approximately constant; consequently the analysis can be simplified by reporting upper limits per unit volume per unit time. During the current analysis, the sensitivity of the detectors to the systems of interest (as shown in Figure 2) was sufficiently large that we could assume signals were uniformly distributed in volume. We therefore quote upper limits in units of $\text{Mpc}^{-3}\text{yr}^{-1}$. To incorporate the previous results as prior distributions, we converted from L_{10} to Mpc^3 using a conversion factor of $0.02 L_{10}$ per Mpc^3 [25].

We estimate the volume to which the search is sensitive by reanalyzing the data with the addition of a large number of simulated signals (“software injections”) in order to model the source population. Our ability to detect a signal depends upon the parameters of the source, including the component masses, the distance to the binary, its sky location, and its orientation with respect to the detectors. Numerous signals with randomly chosen parameters were therefore injected into the data. To compute the sensitive volume for a given binary mass, we perform a Monte Carlo integration over the other parameters to obtain the efficiency of the search—determined by the fraction of simulated signals found louder than the loudest foreground event—as a function of distance. Integrating the efficiency as a function of distance then gives the sensitive volume.

We consider several systematic uncertainties that limit the accuracy of the measured search volume and therefore the upper limits [10]: detector calibration errors (conservatively estimated to be 14% in sensitive distance combined over all three detectors and over the entire observational period, and a 2% bias correction), waveform errors (taken to be a one-sided 10% [22] bias towards lower sensitive distance), and Monte Carlo statistical errors (3-5% in sensitive volume). We convert the sensitive distance uncertainties to volume uncertainties, and then marginalize over the uncertainty in volume to obtain an upper limit which takes into account these systematic uncertainties [22].

In Table I we present the marginalized upper limits at the 90% confidence level assuming canonical mass distributions for non-spinning BNS ($m_1 = m_2 = 1.35 \pm 0.04 M_\odot$), BBH ($m_1 = m_2 = 5 \pm 1 M_\odot$), and NSBH

System	BNS	NSBH	BBH
Component masses (M_\odot)	1.35 / 1.35	1.35 / 5.0	5.0 / 5.0
D_{horizon} (Mpc)	40	80	90
Non-spinning upper limit ($\text{Mpc}^{-3}\text{yr}^{-1}$)	1.3×10^{-4}	3.1×10^{-5}	6.4×10^{-6}
Spinning upper limit ($\text{Mpc}^{-3}\text{yr}^{-1}$)	...	3.6×10^{-5}	7.4×10^{-6}

TABLE I: Rate upper limits of BNS, BBH and NSBH coalescence, assuming canonical mass distributions. D_{horizon} is the horizon distance averaged over the time of the search. The sensitive distance averaged over all sky locations and binary orientations is $D_{\text{avg}} \simeq D_{\text{horizon}}/2.26$ [26]. The first set of upper limits are those obtained for binaries with non-spinning components. The second set of upper limits are produced using black holes with a spin uniformly distributed between zero and the maximal value of Gm^2/c .

($m_1 = 1.35 \pm 0.04 M_\odot$, $m_2 = 5 \pm 1 M_\odot$) systems. We also compute upper limits as a function of total mass M , using an injection population distributed uniformly over M and uniformly over m_1 for a given M . For NSBH systems we present the upper limit as a function of black hole mass, keeping the neutron-star mass fixed in the range $1 - 3 M_\odot$. These are presented in Figure 4. Figure 5 compares the upper limits obtained in this analysis (dark gray regions) to limits obtained in our previous searches up to S5/VSR1 [4] (light gray region) and to astrophysically-predicted rates (blue regions) for BNS, NSBH, and BBH systems. The improvement over the previous limits is up to a factor of 1.4, depending on binary mass; this reflects the additional observation time and improved sensitivity of the S6/VSR2/VSR3 data with respect to all previous observations.

Although we searched with a bank of non-spinning templates, we compute upper limits for NSBH and BBH systems in which one or both of the component masses are spinning. These results are also presented in Table I. We did not compute upper limits for spinning BNS systems because astrophysical observations indicate that neutron stars cannot have large enough spin to significantly affect waveforms observable in the LIGO frequency band [27, 28]. Black hole spins were uniformly distributed in both orientation and magnitude, S , with S constrained to the range $0 \leq S \leq Gm^2/c$, and m is the mass of the black hole. As can be seen in Table I, the spinning upper limits are $\sim 16\%$ larger than non-spinning. Signals from spinning systems are recovered with a worse match to our templates since we use a non-spinning template bank.

While the rates presented here represent an improvement over the previously published results from earlier LIGO and Virgo science runs, they are still above the astrophysically predicted rates of binary coalescence. There are numerous uncertainties involved in estimating astrophysical rates, including limited numbers of observations and unknown model parameters; consequently the rate estimates are rather uncertain. For

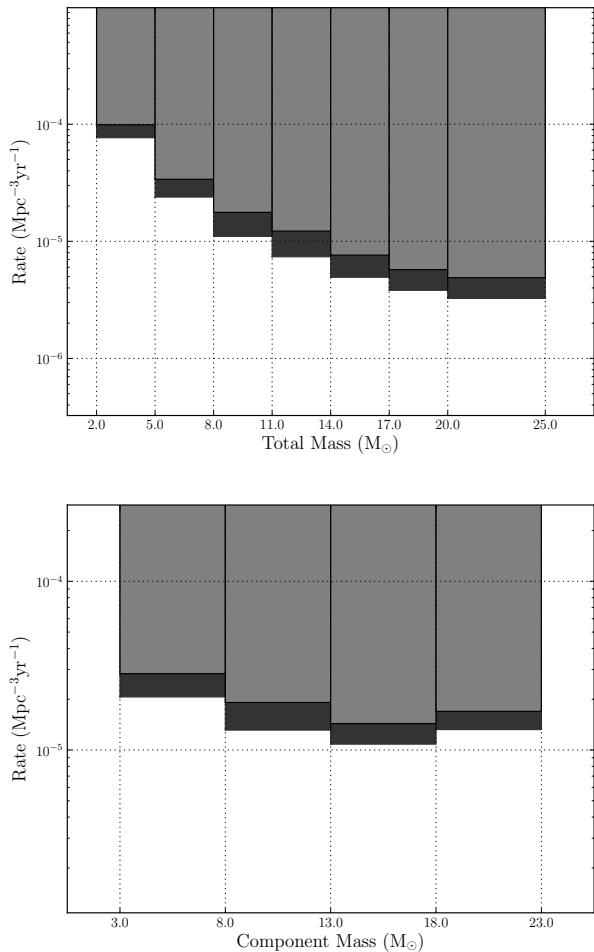


FIG. 4: The marginalized upper limits as a function of mass. The top plot shows the limit as a function of total mass M , using a distribution uniform in m_1 for a given M . The lower plot shows the limit as a function of the black hole mass, with the neutron star mass restricted to the range $1 - 3 M_{\odot}$. The light bars indicate upper limits from previous searches. The dark bars indicate the combined upper limits including the results of this search.

BNS systems the estimated rates vary between 1×10^{-8} and $1 \times 10^{-5} \text{Mpc}^{-3}\text{yr}^{-1}$, with a “realistic” estimate of $1 \times 10^{-6} \text{Mpc}^{-3}\text{yr}^{-1}$. For BBH and NSBH, realistic estimates of the rate are $5 \times 10^{-9} \text{Mpc}^{-3}\text{yr}^{-1}$ and $3 \times 10^{-8} \text{Mpc}^{-3}\text{yr}^{-1}$ with at least an order of magnitude uncertainty in either direction [5]. In all cases, the upper limits derived here are two to three orders of magnitude above the “realistic” estimated rates, and about a factor of ten above the most optimistic predictions. These results are summarized in Figure 5.

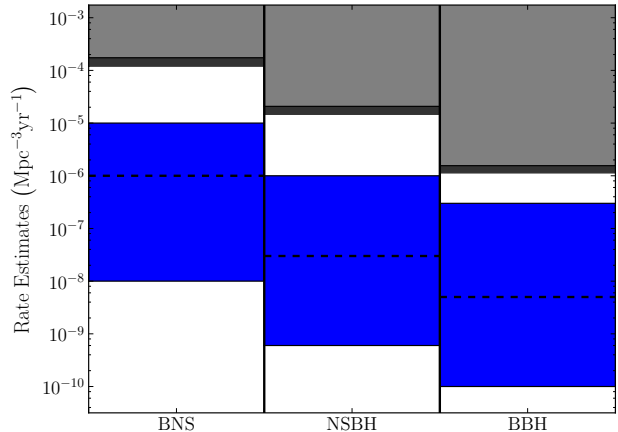


FIG. 5: Comparison of CBC upper limit rates for BNS, NSBH and BBH systems. The light gray regions display the upper limits obtained in the S5-VSR1 analysis; dark gray regions show the upper limits obtained in this analysis, using the S5-VSR1 limits as priors. The new limits are up to a factor of 1.4 improvement over the previous results. The lower (blue) regions show the spread in the astrophysically predicted rates, with the dashed-black lines showing the “realistic” estimates [5]. *Note:* In [5], NSBH and BBH rates were quoted using a black-hole mass of $10 M_{\odot}$. We have therefore rescaled the S5 and S6 NSBH and BBH upper limits in this plot by a factor of $(\mathcal{M}_5/\mathcal{M}_{10})^{5/2}$, where \mathcal{M}_{10} is the chirp mass of a binary in which the black hole mass is $10 M_{\odot}$ and \mathcal{M}_5 is the chirp mass of a binary in which the black hole mass is $5 M_{\odot}$.

VII. DISCUSSION

We performed a search for gravitational waves from compact binary coalescences with total mass between 2 and $25 M_{\odot}$ with the LIGO and Virgo detectors using data taken between July 7, 2009 and October 20, 2010. No gravitational waves candidates were detected, and we placed new upper limits on CBC rates. These new limits are up to a factor of 1.4 improvement over those achieved using previous LIGO and Virgo observational runs up to S5/VSR1 [4], but remain two to three orders of magnitude above the astrophysically predicted rates.

The installation of the advanced LIGO and Virgo detectors has begun. When operational, these detectors will provide a factor of ten increase in sensitivity over the initial detectors, providing a factor of ~ 1000 increase in the sensitive volume. At that time, we expect to observe tens of binary coalescences per year [5].

In order to detect this population of gravitational wave signals, we will have to be able to confidently discriminate it from backgrounds caused by both stationary and transient detector noise. It is customary [5] to assume that a signal with SNR 8 in each detector would stand far enough above background that we would consider it to be a detection candidate. The blind injection had somewhat larger SNR than 8 in each detector, and we were able estimate a FAR of 1 in 7000 years for that event.

Alternatively, consider a coincident signal with exactly SNR 8 in two detectors. Provided the signal is a good match to the template waveform ($\chi_r^2 \approx 1$ in equation 1) this corresponds to $\rho_c = 11.3$. As can be seen from the extended background events with the blind injection removed in Figure 3 (light-gray crosses), this gives a FAR of ~ 1 in 2×10^4 years in a single trial, or 1 in 3000 years over all trials. Achieving similar-or-better background distributions in Advanced LIGO and Virgo will require detailed data quality studies of the detectors and feedback from the CBC searches, along with well-tuned signal-based vetoes. We have continued to develop the pipeline with these goals in mind. For this analysis we significantly decreased the latency between taking data and producing results, which allowed data quality vetoes to be finely tuned for the CBC search. These successes, along with the successful recovery of the blind injection, give us confidence that we will be able to detect gravitational waves from CBCs at the expected rates in Advanced LIGO and Virgo.

Acknowledgments: The authors gratefully acknowledge the support of the United States National Science Foundation for the construction and operation of the LIGO Laboratory, the Science and Technology Facilities Coun-

cil of the United Kingdom, the Max-Planck-Society, and the State of Niedersachsen/Germany for support of the construction and operation of the GEO600 detector, and the Italian Istituto Nazionale di Fisica Nucleare and the French Centre National de la Recherche Scientifique for the construction and operation of the Virgo detector. The authors also gratefully acknowledge the support of the research by these agencies and by the Australian Research Council, the International Science Linkages program of the Commonwealth of Australia, the Council of Scientific and Industrial Research of India, the Istituto Nazionale di Fisica Nucleare of Italy, the Spanish Ministerio de Educación y Ciencia, the Conselleria d'Economia Hisenda i Innovació of the Govern de les Illes Balears, the Foundation for Fundamental Research on Matter supported by the Netherlands Organisation for Scientific Research, the Polish Ministry of Science and Higher Education, the FOCUS Programme of Foundation for Polish Science, the Royal Society, the Scottish Funding Council, the Scottish Universities Physics Alliance, The National Aeronautics and Space Administration, the Carnegie Trust, the Leverhulme Trust, the David and Lucile Packard Foundation, the Research Corporation, and the Alfred P. Sloan Foundation.

-
- [1] B. Abbott et al. (LIGO Scientific Collaboration), Rept. Prog. Phys. **72**, 076901 (2009), arXiv:0711.3041.
 - [2] F. Acernese et al., Class. Quant. Grav. **25**, 184001 (2008).
 - [3] LIGO Scientific Collaboration and Virgo Collaboration, The LIGO / Virgo Blind Injection GW100916 (2011), URL <http://www.ligo.org/science/GW100916/>.
 - [4] J. Abadie et al. (LIGO Scientific Collaboration and Virgo Collaboration), Phys. Rev. D **82**, 102001 (2010), arXiv:1005.4655.
 - [5] J. Abadie et al. (LIGO Scientific Collaboration and Virgo Collaboration), Class. Quant. Grav. **27**, 173001 (2010).
 - [6] R. Adhikari, P. Fritschel, and S. Waldman, Tech. Rep. LIGO-T060156-v1, LIGO Project (2006), URL <https://dcc.ligo.org/cgi-bin/DocDB/ShowDocument?docid=7384>.
 - [7] J. Smith (for the LIGO Scientific Collaboration), Classical and Quantum Gravity **26**, 114013 (2009).
 - [8] T. Fricke et al. (2011), arXiv:1110.2815, submitted to Class. Quant. Grav.
 - [9] M. Lorenzini (for the Virgo Collaboration), Class. Quant. Grav. **27**, 084021 (2010).
 - [10] B. Abbott et al. (LIGO Scientific Collaboration), Phys. Rev. D **79**, 122001 (2009), arXiv:0901.0302.
 - [11] B. Abbott et al. (LIGO Scientific Collaboration), Phys. Rev. D **80**, 047101 (2009).
 - [12] B. Allen, W. G. Anderson, P. R. Brady, D. A. Brown, and J. D. E. Creighton (2011), arXiv:gr-qc/0509116, submitted to Phys. Rev. D.
 - [13] S. Babak, R. Balasubramanian, D. Churches, T. Coke-laer, and B. S. Sathyaprakash, Class. Quant. Grav. **23**, 5477 (2006), gr-qc/0604037.
 - [14] L. Blanchet, T. Damour, B. R. Iyer, C. M. Will, and A. G. Wiseman, Phys. Rev. Lett. **74**, 3515 (1995).
 - [15] L. Blanchet, T. Damour, G. Esposito-Farèse, and B. R. Iyer, Phys. Rev. Lett. **93**, 091101 (2004), gr-qc/0406012.
 - [16] C. Van Den Broeck et al., Phys. Rev. D **80**, 024009 (2009).
 - [17] C. A. K. Robinson, B. S. Sathyaprakash, and A. S. Sengupta, Phys. Rev. D **78**, 062002 (2008).
 - [18] B. Allen, Phys. Rev. D **71**, 062001 (2005).
 - [19] N. Christensen (for the LIGO Scientific Collaboration and the Virgo Collaboration), Class. Quantum Grav. **27**, 194010 (2010).
 - [20] F. Robinet (for the LIGO Scientific Collaboration and the Virgo Collaboration), Class. Quant. Grav. **27**, 194012 (2010).
 - [21] D. M. Macleod, S. Fairhurst, B. Hughey, A. P. Lundgren, L. Pekowsky, J. Rollins, and J. R. Smith (2011), arXiv:1108.0312, submitted to Class. Quant. Grav.
 - [22] P. R. Brady and S. Fairhurst, Class. Quantum Grav. **25**, 105002 (2008), arXiv:0707.2410.
 - [23] P. R. Brady, J. D. E. Creighton, and A. G. Wiseman, Class. Quantum Grav. **21**, S1775 (2004).
 - [24] R. Biswas, P. R. Brady, J. D. E. Creighton, and S. Fairhurst, Class. Quantum Grav. **26**, 175009 (2009), arXiv:0710.0465.
 - [25] R. K. Kopparapu, C. Hanna, V. Kalogera, R. O'Shaughnessy, G. Gonzalez, P. R. Brady, and S. Fairhurst, Astrophys. J. **675**, 1459 (2008).
 - [26] L. S. Finn and D. F. Chernoff, Phys. Rev. D **47**, 2198 (1993), arXiv:gr-qc/9301003.
 - [27] R. N. Manchester, G. B. Hobbs, A. Teoh, and M. Hobbs, Astronom. J. **129**, 1993 (2005).
 - [28] T. A. Apostolatos, C. Cutler, G. J. Sussman, and K. S. Thorne, Phys. Rev. D **49**, 6274 (1994).